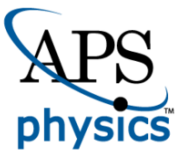

Self-acceleration and global pulsation in expanding laminar H_{2}-O_{2}-N_{2} flames

Jialong Huo, Abhishek Saha, Tao Shu, Zhuyin Ren, and Chung K. Law

Phys. Rev. Fluids **4**, 043201 — Published 16 April 2019

DOI: 10.1103/PhysRevFluids.4.043201

Self-acceleration and Global Pulsation in Expanding Laminar $H_2/O_2/N_2$ Flames

Jialong Huo[a], Abhishek Saha[b], Tao Shu[a], Zhuyin Ren[a, *], Chung K. Law[b,a]

a) Center for Combustion Energy, Tsinghua University, Beijing 100084, China

b) Department of Mechanical and Aerospace Engineering, Princeton University, Princeton, NJ 08544, USA

Submitted to **Physical Review Fluids**

Article type: Regular Article

*Corresponding author:

E-mail: zhuyinren@tsinghua.edu.cn

ABSTRACT

We report herein the quantitative data and physical insights acquired on the self-acceleration and global pulsation of spherically expanding $H_2/O_2/N_2$ flames, propagating in a constant-pressure environment and subjected to hydrodynamic and diffusional-thermal instabilities over a wide range of pressures and equivalence ratios. Results show that the critical radii for the onset of the transition stage and global pulsation stage have a similar variation with pressure and equivalence ratio, and can be collapsed by plotting the nondimensional values normalized by the planar flame thickness. Furthermore, through experiments with fixed flame temperature achieved by adjusting the amount of N_2 in air, it is demonstrated that the global pulsation frequencies dominated by the diffusional-thermal instability increase with its intensity, which is consistent with the hypothesis that the global pulsation behavior of cellular flames arises from the continuous cell growth and splitting during the flame propagation. The global pulsation frequencies of H_2/air flames, subjected to the coupled hydrodynamic and diffusional-thermal instabilities, show a non-monotonic trend with the equivalence ratio; while their nondimensional values, normalized by the flame time, collapse and decrease with increasing equivalence ratio, in that the pressure and flame temperature effects are properly scaled out through the normalization. The acceleration exponents of the transition stage and global pulsation stage are also determined, with the latter slightly smaller than the critical value of 1.5 suggested for self-turbulization.

Keywords: self-acceleration; flame-front instability; global pulsation; expanding laminar flame

I. INTRODUCTION

A propagating premixed flame is subjected to two intrinsic modes of cellular instabilities, namely the Darrieus-Landau (DL) hydrodynamic instability and the diffusional-thermal (DT) instability. Mechanistically, the DL instability is induced through the sharp density change across the flame-front and is facilitated either for large flame dimensions, for which the flame is much thinner than the hydrodynamic scale of the flow field, or in a high-pressure environment because of the increased reaction rate and hence reduced flame thickness [1-5]. On the other hand, the DT instability is controlled by the imbalances in the diffusivities of the masses of the various species and of heat, conventionally characterized by a global Lewis number, *Le*, defined as the ratio of the thermal diffusivity of the mixture to the mass diffusivity of the controlling and thus deficient reactant. In particular, the DT cellular instability is promoted for $Le < 1$ mixtures and suppressed otherwise [2, 3, 5-7]. Furthermore, due to the coexistence of the DL instability, unless the flame is relatively thick, and the DT instability, unless the mixture *Le* is close to unity, special considerations in terms of the mixture properties and experimental conditions are needed to isolate and separately study the manifestation of these two modes of instabilities.

We next note that the continuous evolution of cells over a flame surface, especially if it is globally expanding, could lead to a concomitant steady increase in the global flame propagation speed and the heat release rate. This phenomenon has been termed self-acceleration and has been extensively studied theoretically [1-3, 6-8] and experimentally [4, 9-17]. Furthermore, it has been recently shown through experiments [18] and simulations [19, 20] that self-acceleration of these flames can globally pulsate between states of faster and slower acceleration, with the latter case even occasionally exhibiting deceleration. This discovery has generated considerable interest because of its fundamental significance

in the generation of pulsatory instability through the nonlinear interaction of spatial cells, and practical significance in the potential induction of combustion instability within burners. In particular, a rational study on the generation and characteristics of pulsating propagation has been conducted [21] for the DL instability through experimentation with diffusionally neutral, *Le*~1, mixtures in high and constant pressure environments, with the concomitant determination of the frequency and acceleration exponent of the pulsatory multi-stage acceleration.

The present study then aims to extend the work of [21] by experimentally investigating the separate role of the DT cells, as well as its coupled role with the DL cells, in the generation of global pulsation, and as such provides a comprehensive characterization and data base for these newly discovered global pulsation phenomena. Specifically, we shall present an experimental study of lean, stoichiometric and rich mixtures of H_2, O_2 and N_2, and quantify the influence of the Lewis number on the characteristics of global pulsation, and to investigate the coupled and decoupled effects of the DL and DT cellular instabilities on the manifestation of this global pulsation; noting herein that since the burned flame temperature can be fixed at a certain value by adjusting the amount of N_2 in the mixture, the effects of DL and DT instabilities can be unambiguously isolated. Finally, we shall also explore the possibility of unifying the observed pulsation frequencies using fundamental flame parameters.

II. EXPERIMENTAL METHODOLOGIES

The experiments were conducted in a constant-pressure dual-chambered vessel, reported in [22]. The combustible mixture was introduced into the inner chamber based on the partial pressure of each species, while the outer chamber is filled with an inert at the same pressure. Ignition energy is deposited by a spark at the center of the inner chamber via electrodes extending from opposite locations, resulting in an outwardly expanding flame. The evolution of the flame-front morphology was imaged

using Schlieren photography and recorded with a high-speed digital camera (Photron Fastcam SA-Z), yielding the instantaneous flame radius $R_f(t)$, defined as $R_f = \sqrt{\int_0^{2\pi} R_L^2 d\theta/\pi}$, where $R_L(\theta)$ is the local flame radius from the center and hence is a function of angle θ. The subsequent instantaneous flame speed, based on the burned mixture, is $S_b(t)=dR_f(t)/dt$. Images were taken at 20,000 frames per second (fps) with 1024×1024 pixels for $P \leq 4.0$ atm, and at 60,000 fps with 512×512 pixels for $P = 5.0$ atm. The spatial resolution is roughly 0.2 mm/pixel.

Two sets of experimental conditions were conducted, using H_2 as the fuel. In the first set, H_2/air flames at $0.6 \leq \phi \leq 1.1$ and 1.0 atm $\leq P \leq$ 5.0 atm were used to study the coupled DL and DT instabilities. In addition, we also investigated the individual role of the DT instability by working with experimental conditions of H_2 flames listed in Table 1, where the burned temperature is fixed at 1800 K by adjusting the amount of N_2 in air. Consequently, the contributions of hydrodynamic instability to the wrinkling behavior are nearly identical and the effects of DT instability can be accentuated/mitigated by making the mixture leaner/richer.

Table 1

ϕ: equivalence ratio; T_b: adiabatic flame temperature; P: pressure; X_i: mole fraction of species i, i = H_2, O_2 and N_2; δ_f: flame thickness based on temperature gradient; σ: thermal expansion ratio; Le: Lewis number. Initial temperature is 298 K.

ϕ	T_b (K)	P (atm)	X_{H_2}	X_{O_2}	X_{N_2}	δ_f(mm)	S_b^0 (cm/s)	Le
0.6			0.197	0.164	0.639	0.121	315.2	0.45
0.7			0.197	0.140	0.663	0.128	308.9	0.50
0.8	1800	3	0.196	0.123	0.681	0.136	302.2	0.58
0.9			0.196	0.109	0.695	0.142	295.4	0.68
1.0			0.197	0.098	0.705	0.147	296.1	0.81

The effective Lewis number in Table 1 is calculated as [8]

$$Le = [1+(Le_E-1)+\mathcal{A}(Le_D-1)]/(1+\mathcal{A})$$

where $\mathcal{A} = 1 + Ze(\Phi - 1)$ measures the mixture's strength, Φ is defined as the ratio of the mass of excess to deficient reactants in the fresh air relative to their stoichiometric ratio, $Ze = E_a(T_b-T_u)/R^0T_b^2$ is the

Zel'dovich number, E_a the global activation energy, and R^0 the gas constant. In the present work, E_a/R^0 is evaluated by assessing the change in the reaction rate due to small variations of the amount of N_2 in the mixture, hence flame temperature.

III. FLAME-FRONT EVOLUTION AND CRITICAL RADIUS

A set of high-speed images of experimentally observed expanding flames at different pressures and equivalence ratios are shown in Fig. 1. It is seen from column A that, while the flame-front at $\phi = 0.6$ and $P = 1.0$ atm is stable, hence smooth, at small radius ($R_f < 2.0$ cm), except for the large-scale cracks generated from electrodes, cellular structure is visible at larger flame sizes. Furthermore, since the DL instability is enhanced as the pressure increases through reduced flame thickness, the flame morphologies in columns B and E show that the cellular structure appears earlier at higher pressures. Figure 2 further shows the fronts of the flames in Columns B, C, and D in Fig. 1 at $R_f = 1.0$ cm, 3.0 cm and 5.0 cm, demonstrating that the flame-front indeed becomes less wrinkled, which indicates that the DT instability becomes weaker, with increasing equivalence ratio, which directly enhances *Le*.

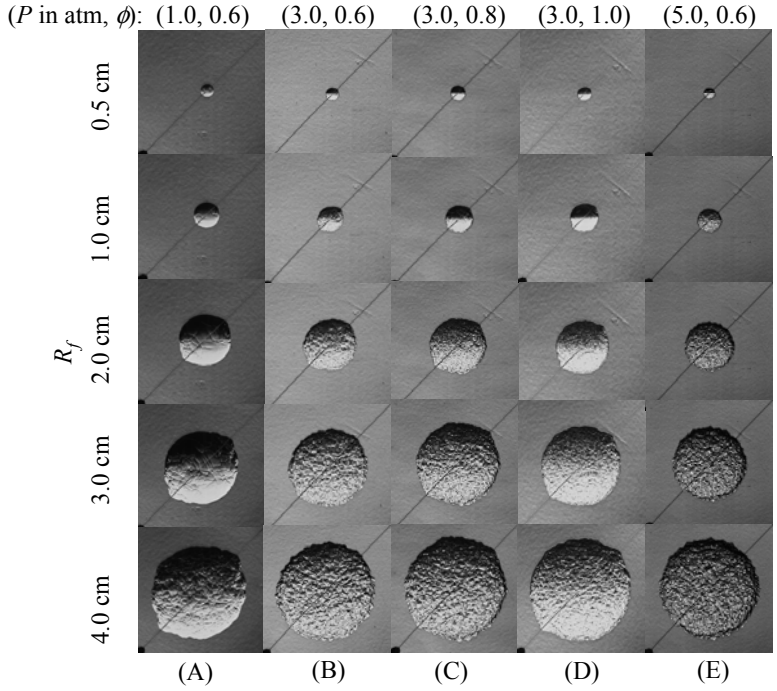

FIG. 1. Schlieren images from the spherical flame propagation of H_2/air flames at different pressures and equivalence ratios.

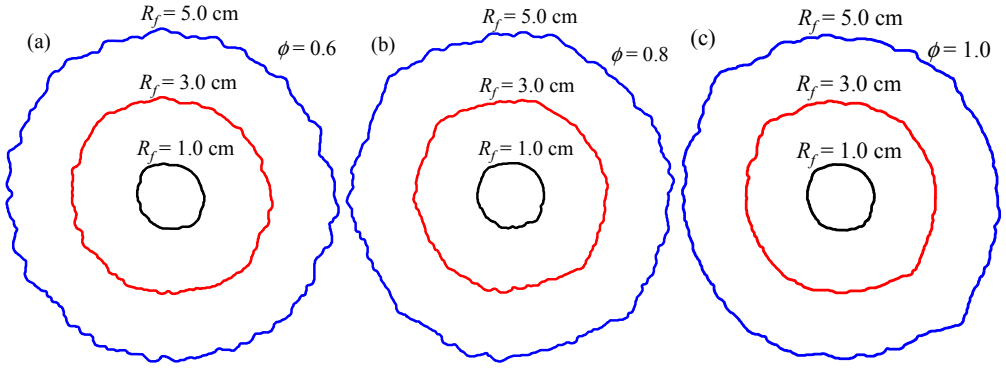

FIG. 2. Flame-fronts of H_2/air flames at different equivalence ratios. P = 3.0 atm. (a) ϕ = 0.6, (b) ϕ = 0.8, (c) ϕ = 1.0.

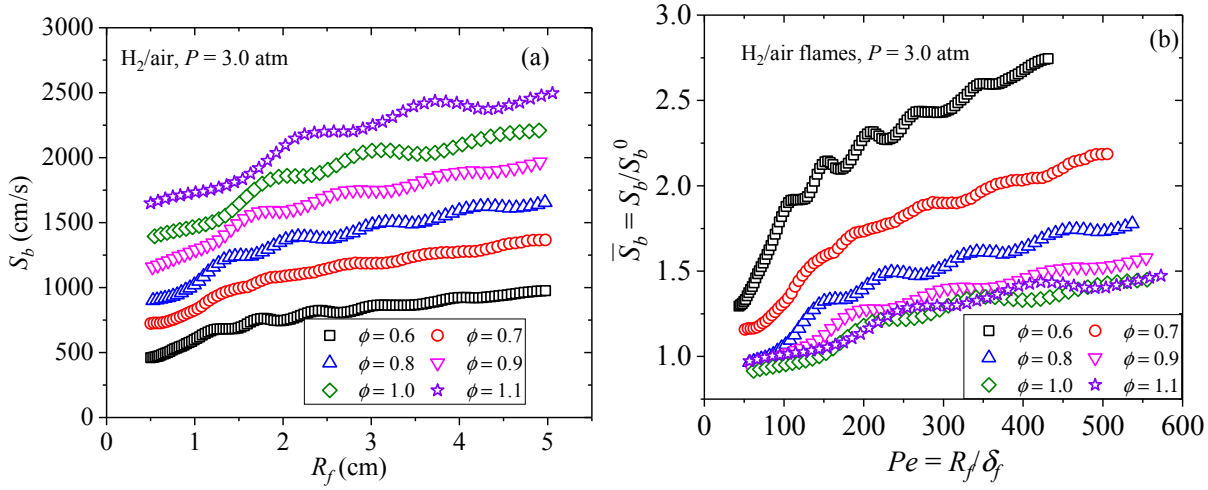

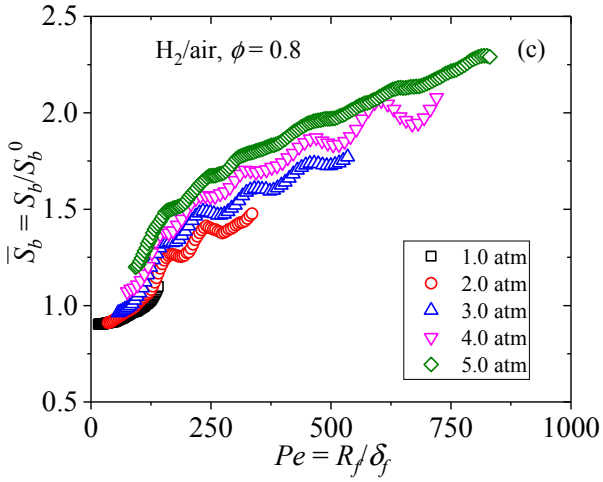

FIG. 3. Propagation of cellular flames with pulsatory behavior for H_2/air flames at P = 3.0 atm and 0.6 ≤ ϕ ≤ 1.1. T_u = 298K. (a) dimensional flame speed, S_b vs. flame radius, R_f; (b) normalized flame speed, $\bar{S}_b = S_b/S_b^0$ vs. normalized flame radius or Peclet number, $Pe = R_f/\delta_f$, where $\delta_f = (T_b\text{-}T_u)/(dT/dx)_{max}$ is the flame thickness; (c) $\bar{S}_b$ vs. Pe for H_2/air flames at ϕ = 0.8 and pressures is from 1.0 atm to 5.0 atm.

To assess the role of DT instability on cellular flames, we next present in Figs. 3(a) the measured downstream burned flame speeds, S_b, of H_2/air flames at P = 3 atm, in the range of Le or equivalence ratio (0.6 ≤ ϕ ≤ 1.1), as a function of the flame radius, R_f. It is evident that the flame propagates faster as ϕ increases, which is a combined effect of the intensity of the DT instability and the flame temperature, in that the former is weakened with increasing ϕ due to the larger Le, while the latter is enhanced as the flame becomes richer and thus the chemical reactivity is increased. To largely scale out the influence of the flame temperature on flame propagation, in Fig. 3(b) S_b is normalized with the unstretched planar laminar flame speed, S_b^0, and plotted with the nondimensional radius, or the Peclet number, defined as $Pe = R_f/\delta_f$. Here S_b^0 is calculated from the CHEMKIN Premixed code using the H_2/O_2 mechanism from Burke et al. [23]. Additionally, we have also plotted the normalized flame speed for a fixed equivalence ratio (ϕ = 0.8), but at various pressures (1.0 atm ≤ P ≤ 5.0 atm) to identify the pressure effect on flame acceleration. Several key features can be observed from the global flame images and nondimensional propagation speeds. First, the presence of global pulsation in the

propagation of cellularly unstable flames is clearly visible through the oscillations of the flame speed in both dimensional and nondimensional plots (Figs. 3(a) and (b), (c)) respectively. Second, for a fixed equivalence ratio, and for lower pressure or smaller flame radius, represented by a small *Pe*, flame propagation is devoid of any instabilities, as shown by the smooth flame-front for $\phi = 0.6$ at $P = 1.0$ atm in column A in Fig. 1 for $R_f < 2.0$ cm. At this smooth flame-front stage, the propagation is affected by flame stretch alone. As the flame grows large enough such that the flame radius exceeds a critical value, R_{ct}, flame-front instability is triggered and cells start to appear over the entire flame-front [24]. The appearance of cells causes the flame to accelerate rapidly through the excess flame area generated. This stage will be referred to as the transition stage. As the flame continues to grow and reaches another critical radius, R_{cp}, the flame either accelerates with reduced magnitude or even decelerates, demonstrating the oscillatory nature of the propagation. The acceleration and deceleration of the flame will then repeat themselves, resulting in global pulsation. This stage will be referred as the global pulsation stage.

Since the criterion at which a freely propagating expanding flame becomes cellularly unstable can be characterized by the critical radii mentioned above, we now discuss the effects of pressure and equivalence ratio on this criticality. Figure 4(a) shows the critical flame radius for the onset of the transition stage, R_{ct}, for H_2/air flames at different pressures and equivalence ratios. It is seen that, for H_2/air flames at fixed ϕ, R_{ct} decreases as pressure increases, which has also been reported for $Le = 1$ flames in our previous work [21]. Recognizing that this decrease in R_{ct} with increasing pressure results from the increased intensity of hydrodynamic instability, and that increased pressure enhances the chemical reactivity and hence reduces the flame thickness, the normalized critical flame radius $Pe_{cp} = R_{cp}/\delta_f$ is plotted in Fig. 4(b) to eliminate the pressure induced effects, where $\delta_f = (T_b - T_u)/(dT/dx)_{\max}$ is the flame thickness. In particular, we note that for any given equivalence ratio, Pe_{ct} is fairly insensitive

to pressure variations. This effect has been discussed in [3, 8], which suggests that Pe_{ct} is a function of thermal expansion (σ) and Lewis number (Le) of the flame as $Pe_{ct} = Pe_1(\sigma) + Ze(Le\text{-}1)Pe_2(\sigma)$ [13]. The first term of this expression, $Pe_1(\sigma)$, represents the effect of pure hydrodynamic or Darrieus-Landau instability, while the second term, $Ze(Le\text{-}1)Pe_2(\sigma)$, provides the stabilization or destabilization effect of diffusional-thermal instability through the Le. Since both β and σ are insensitive to pressure for H_2/air flames, Pe_{ct} should also be insensitive to pressure, as observed in Fig. 4(b). It is also seen that with increasing equivalence ratio, R_{ct} and Pe_{ct} shift to larger values due to the increase in Le and thus corresponding stabilizing intensity, which is consistent with the theory. The results are also consistent with the findings of Jomaas et al. [13]. Here we note that to avoid effects of ignition on the determination of R_{ct}, we have intentionally used the minimum possible ignition energy.

Although the critical radius (or Peclet number) for the inception of instability has been reported and investigated extensively in the literature, the associated critical radius (or Peclet number) for the onset of global pulsation has not been reported before, since the global pulsation of expanding cellularly unstable flame is a fairly new phenomenon observed in experiments. In Fig. 5 we report the critical Pe for the onset of the global pulsation stage, Pe_{cp}, measured for H_2/air flames at different pressures and equivalence ratios. It is seen that Pe_{cp} is larger than Pe_{ct} under all the experimental conditions, as should be the case. Furthermore, we find that Pe_{cp} is also almost a constant across all the pressures, and slightly increases with the equivalence ratio, which is consistent with the findings in [4]. The similarity of Pe_{ct} and Pe_{cp} variation with pressure and equivalence ratio indicates that the onset of the global pulsation stage should be presumably determined by thermal expansion and the Lewis number.

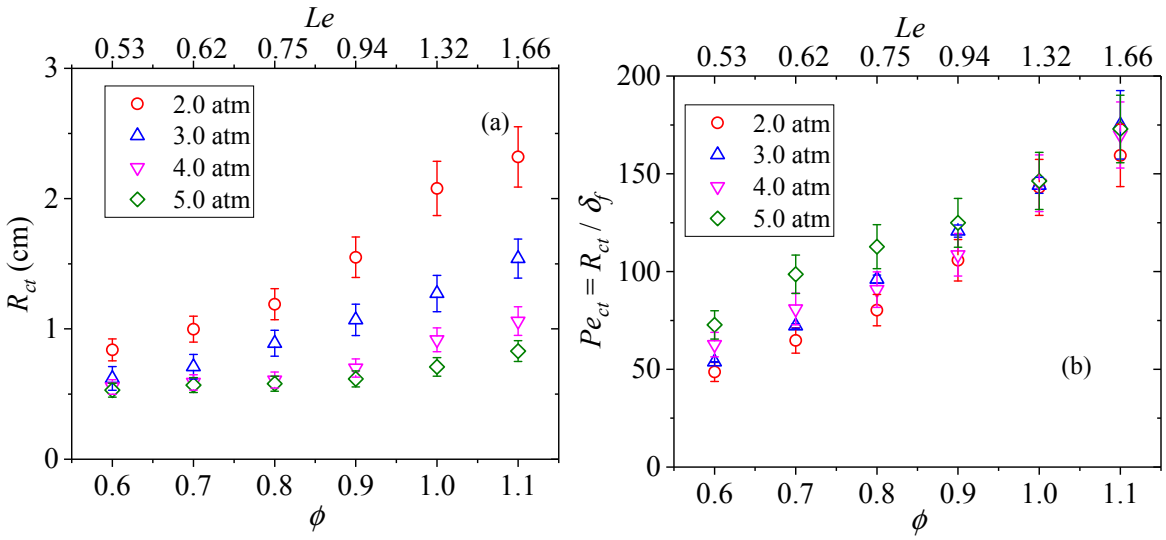

FIG. 4. Critical radius for the onset of the transition stages for H_2/air flames at 2.0 atm $\leq P \leq$ 5.0 atm. 0.6 $\leq \phi \leq$ 1.0. (a) dimensional critical flame radius, R_{ct}; (b) non-dimensional critical flame radius, $Pe_{ct} = R_{ct}/\delta_f$, where $\delta_f = (T_b - T_u)/(dT/dx)_{max}$ is the flame thickness.

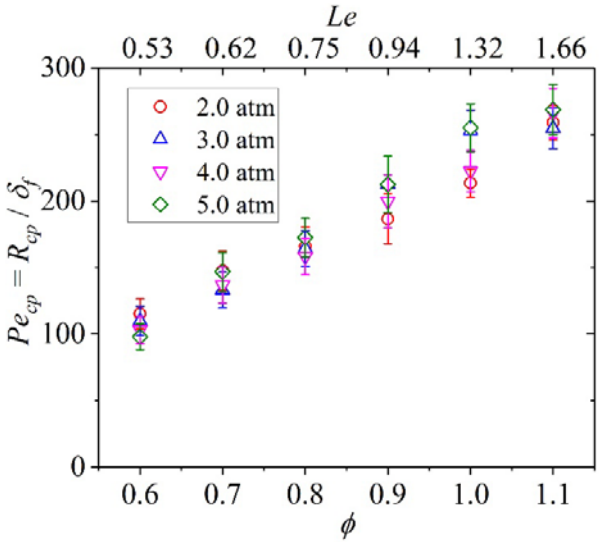

FIG. 5. Critical non-dimensional critical flame radius, ($Pe_{ct} = R_{ct}/\delta_f$) for the onset of the global pulsation stages for H_2/air flames at 2.0 atm $\leq P \leq$ 5.0 atm. 0.6 $\leq \phi \leq$ 1.0.

IV. GLOBAL PULSATION

We next focus on the global pulsation in flame propagation. As stated and shown in previous studies [18, 19], we first hypothesize that while the flame is globally expanding, the global pulsation arises from the continuing growing and splitting of the local cellular structure, causing phases of faster and slower growth in the surface area. Such an intermittently varying local burning rate consequently would

cause the local flame speed to oscillate, even after global averaging, due to nonlinear coupling. As shown by Altantzis et al. [20] and is reasonable to expect, the integrated heat release rate also pulsates as the flame expands. This is qualitatively consistent with the pulsation of the global flame speed, in that the local flame speed is mainly controlled by the flame temperature, *i.e.* the heat release rate, while the global flame speed will in addition also depend on the integrated flame surface area. Furthermore, for flames with higher intensity of flame-front instability, the growth and splitting of the cells would take less time such that the cascading process occurs more often. Consequently, the frequency of the global pulsation should be larger under conditions with stronger flame-front instability. Since the prediction from the hypothesis has partly been validated in our recent work, that the global pulsation frequency increases as the intensity of the hydrodynamic instability becomes stronger (higher pressure or higher flame temperature) [21], we will focus in the following the pure DT instability and the coupling of DL and DT instabilities on the pulsation frequency.

A. Pure DT instability effect

The pure DT instability effect on flame propagation and pulsation is investigated using the experimental conditions in Table 1, where the pressure is 3.0 atm and the $H_2/O_2/N_2$ flame temperature is fixed at 1800 K, by manipulating the amount of N_2 in air, to suppress the DL instability. The intensity of the DT instability is varied by changing the equivalence ratio and can be characterized by the Lewis number. Note that the leaner the mixture, the stronger the DT instability intensity. The dimensional flame speed, *i.e.* S_b vs. R_f, at different equivalence ratios is shown in Fig. 6(a). It is seen that the flame propagation speed decreases and the onset of flame speed acceleration, *i.e.* R_{ct}, is slightly delayed, when the equivalence ratio increases due to weakened DT instability. Nevertheless, the global pulsation of the flame propagation can be observed under all conditions once the flame radius exceeds the critical

values. Figure 6(b) shows the corresponding nondimensional flame propagation speed, namely the normalized flame speed, $\bar{S}_b = S_b/S_b^0$, versus the Peclet number, $Pe = R_f/\delta_f$, demonstrating that the *Pe* range is reduced as the equivalence ratio increases through the increased flame thickness, as listed in Table 1. The equivalence ratio effect on the pulsation frequency, which is characterized by the global pulsation peaks and valleys, is shown in Fig. 7, demonstrating that the frequency monotonously decreases from 1050 Hz to 400 Hz when the equivalence ratio is increased from 0.6 to 1.0. This indicates that purely increasing the intensity of the diffusional-thermal instability will increase the pulsation frequency, which is consistent with the hypothesis.

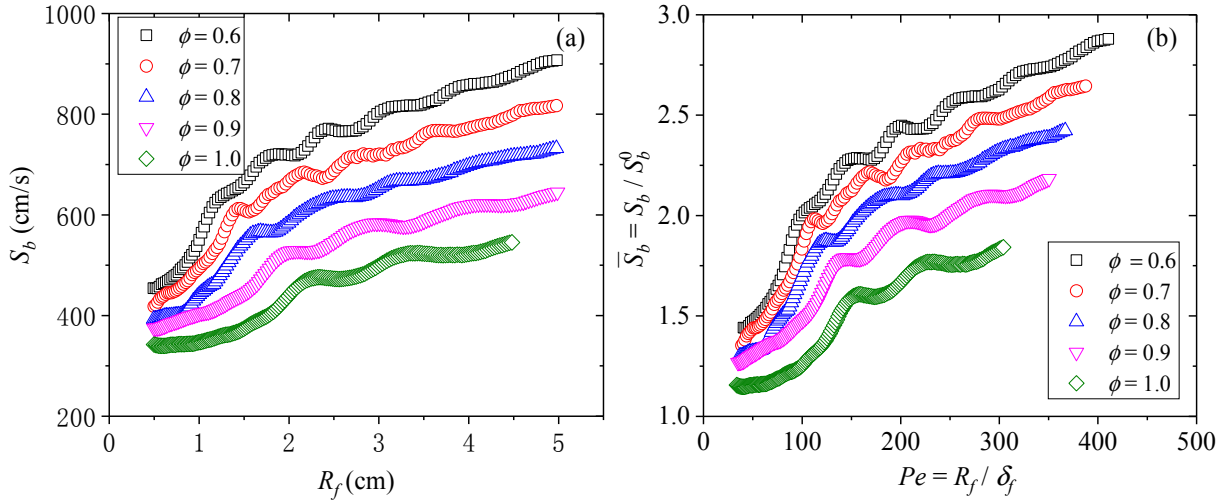

FIG. 6. Propagation of cellular flames with pulsatory behavior for $H_2/O_2/N_2$ flames at $T_u = 298$ K and $P = 3.0$ atm. The experimental conditions are listed in Table 1. The burned flame temperature is fixed at 1800 K by varying the N_2 amount in air. (a) dimensional flame speed, S_b vs. flame radius, R_f; (b) normalized flame speed, $\bar{S}_b = S_b/S_b^0$ vs. normalized flame radius or Peclet number, $Pe = R_f/\delta_f$.

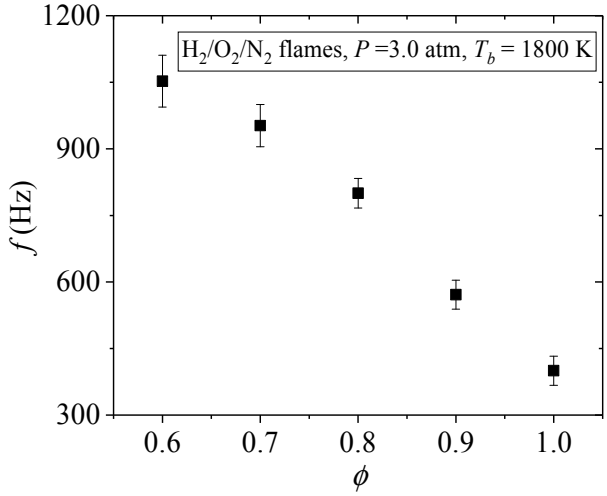

FIG. 7. Frequency, f for global pulsation in $H_2/O_2/N_2$ flames at P = 3.0 atm. The experimental conditions are listed in Table 1.

B. Coupling of hydrodynamic and diffusional-thermal instabilities

Figure 8(a) shows the pulsation frequencies of H_2/air flames at different pressures and equivalence ratios, demonstrating effects of the coupled DL and DT instabilities. It is seen that the pulsation frequency becomes higher as the pressure increases due to the enhanced DL instability. In particular, for all the equivalence ratios, the frequencies at 5.0 atm are almost twice of those at 2.0 atm. Consequently, significantly larger recording rates are required to capture the global pulsation phenomenon at high pressures. For example, at P = 5 atm, it is found that a recording rate of 20,000 fps at 1024×1024 pixel^2 resolution is not sufficient to resolve the behavior and a much greater frame rate of 60,000 fps, at a reduced resolution of 512×512 pixel^2, is required to capture the pulsation.

Moreover, for all the pressures in the present work, f increases and then decreases with ϕ and peeks at around ϕ = 0.8. This non-monotonous variation of f with ϕ is due to the coupled diffusional-thermal and hydrodynamic instabilities. Specifically, as ϕ increases from 0.6 to 1.1, Lewis number of the mixture increases and thus the intensity of the diffusional-thermal instability decreases, while the flame temperature increases and thus the hydrodynamic instability intensity increases. From ϕ = 0.6 to ϕ = 0.8, increase of the hydrodynamic instability intensity dominates such that the pulsation frequency increases.

However, from $\phi = 0.8$ to $\phi = 1.1$, decrease of the diffusional-thermal instability intensity dominates instead, resulting in reduced pulsation frequency.

To identify the proper scaling dependence in the present pulsation phenomena, Fig. 8(b) shows the measured pulsation frequencies normalized with the flame time, defined as δ_f / S_b^0. It is seen that the normalized pulsation frequencies are almost constant across all pressures, and decrease with increasing equivalence ratio, which indicates that effects induced by pressure and flame temperature, *i.e.* DL instability, on the pulsation frequency are properly eliminated. Therefore, the normalized pulsation frequencies are dominated by the DT instability. Figure 8(b) clearly shows that the normalized frequencies decrease with increasing *Le*.

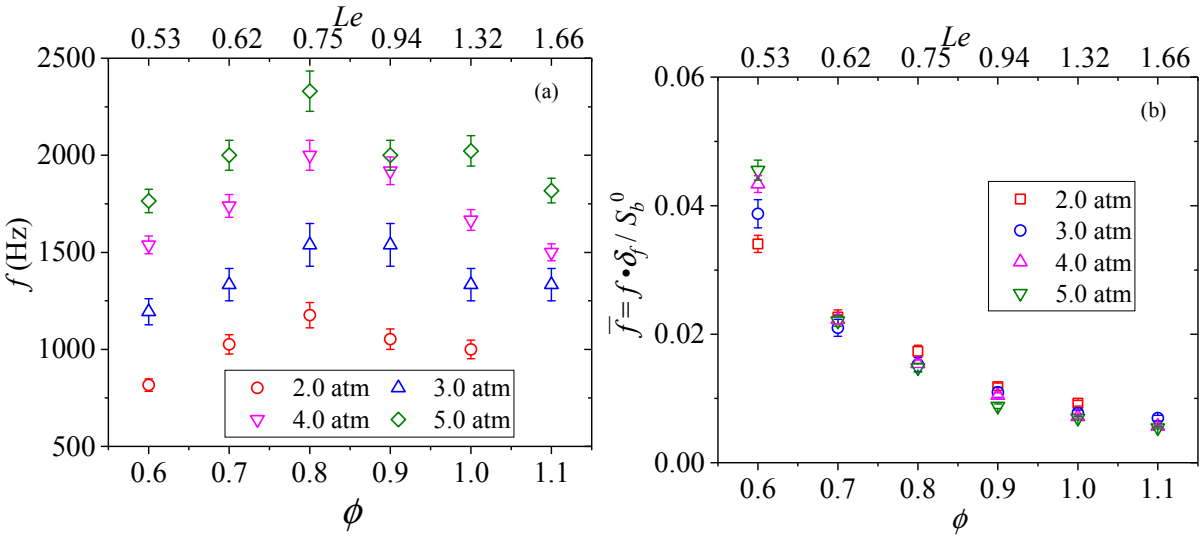

FIG. 8. Global pulsation frequency for H_2/air flames. $0.6 \leq \phi \leq 1.0$ and 2.0 atm $\leq P \leq$ 5.0 atm. (a) dimensional frequency, *f*; (b) non-dimensional frequency, $\bar{f} = f \cdot \delta_f / S_b^0$.

C. Comparisons between experiments and 1D pulsation model

Considering that global pulsation is caused by the ongoing cell growing and splitting, a 1D global pulsation model was proposed by Bauwens *et. al*. [25]. In this model, the growth of each length scale is treated independently. A growth rate relation from linear stability theory and a criterion for cell splitting, based on a critical stretch rate, is used. Global flame surface wrinkling, and overall flame speed, was

obtained through numerical integration of a superposition of the length scales.

An intrinsic assumption of the 1D model is that the behaviors of cells are similar, and thus insensitive to their positions on the flame-front. To validate this assumption, we plot in Fig. 9(a) the flame propagation speed at a fixed angular location, *i.e.* $S_b(\theta) = dR_L(\theta)/dt$. Note that the previously used $S_b = dR_f/dt$ is defined on the total projection area of the Schilieren images and, as such, R_f is an overall average of $R_L(\theta)$. Figure 9(a) shows that the flame propagation speeds along three different radial directions have similar behavior in both the acceleration and deceleration stages. Moreover, the averaged flame propagation speed behaves closely to those at fixed θ. These observations clearly demonstrate that the cells over the flame-front have similar behavior and thus the global pulsation can be interpreted with a 1D model. The results from the 1D model and experiments are compared for H_2/air flames in Figs. 9(b) for ϕ = 1.0 and 1.1. Note the coefficient of the proportionality G^*, the wavenumber of the first-generation cells n_c, are 3.0, 7.0, respectively. It is seen the modeled results exhibit a qualitatively similar trend as the experiments in the flame propagation, indicating that the cell splitting and growing can be properly captured, even the model is 1D.

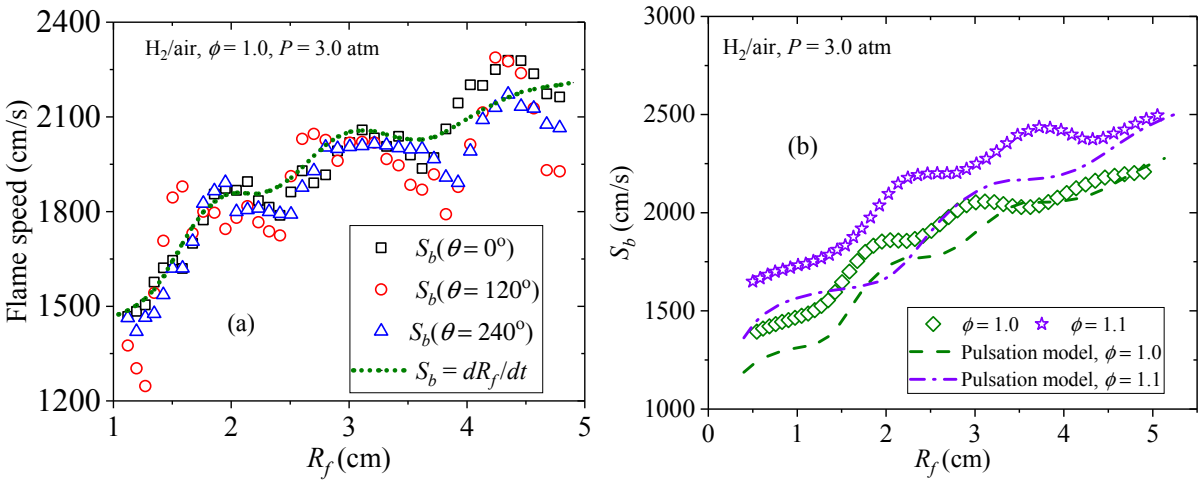

FIG. 9. The flame propagation speed along a certain angle, $S_b(\theta) = dR_L(\theta)/dt$. The experimental condition is stoichiometric H_2/air flame. P = 3.0 atm. G^* = 3.0 and n_c = 7.0 for both ϕ = 1.0 and 1.1 in

(b).

V. ACCELERATION EXPONENTS

It is also of interest to determine the possible values of the acceleration exponent, α, defined through $R_f \approx t^{\alpha}$, which can be further reduced to $S_b = dR_f/dt \approx t^{\alpha-1} \approx R^d$. Here we note that it has been suggested that self-accelerating flames due to cellular instability have the potential for self-turbulization, a state in which the flame propagation mimics that of turbulent flame without any external turbulence-generating source. Since self-accelerating flames and turbulence are often described using fractal models, the exponent $d = 1 - \alpha^{-1}$, termed the fractal excess, can be used to assess if self-turbulization could be achieved [26]. It is noted that, although the DT instability does not display fractal behavior in planar flames [27], propagation speeds of expanding flame can be expressed as a power law, for both DT and DL instabilities, due to the continuing increasing hydrodynamic length scale (flame radius) [14, 15, 18].

Since there is no pulsation in the transition stage, α_t is directly obtained with the formula $S_b = At^{\alpha-1}$. However, in global pulsation, recognizing that the pulsatory behavior would impose a waveform on the otherwise monotonically growing flame speed, we can model the propagation as $S_b = At^{\alpha-1} + Bsin(2\pi ft + \lambda)$, where f and λ are the frequency and phase difference, A and B are constants; and evaluate the values of the acceleration parameters. The determined acceleration exponents of the H_2/air flames for the transition stage (α_t) and the global pulsation stage (α_p) are shown respectively in Figs. 10(a) and 10(b). It is seen that α_t and α_p are insensitive to the equivalence ratio, indicating that the rapid and significant flame acceleration is mainly dominated by the growth of the hydrodynamic cells. Most of the α_t values are between 1.5-1.8, which is consistent with those in [4]. Furthermore, we note that the values of α_p lie between 1.2-1.4, which is slightly smaller than 1.5, the value suggested as the

acceleration exponent for self-turbulization [28].

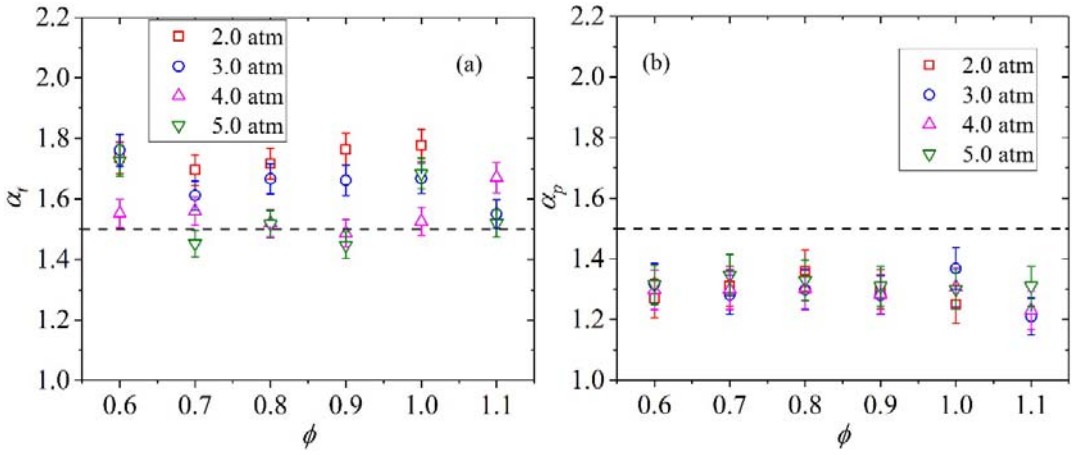

FIG. 10. Acceleration exponent for H_2/air flames at $0.6 \le \phi \le 1.0$ and 2.0 atm $\le P \le$ 5.0 atm. (a) transition stage, α_t; (b) global pulsation stage, α_p.

VI. CONCLUDING REMARKS

In the present study we have investigated the self-acceleration and global pulsation phenomena in the propagation of expanding spherical H_2 flames with flame-front instabilities. It is found that the measured critical flame radii for the onset of the transition stage (R_{ct}) and global pulsation stage (R_{cp}) decrease with increasing pressure and decreasing equivalence ratio, while the non-dimensional values normalized by the flame thickness are almost a constant across all the pressures. In the global pulsation stage, the acceleration and deceleration of the flame propagation speed show an oscillating propagation, which is caused by the continuing growth and splitting of the cellular structures. The effects of the DT and the coupled DL and DT instabilities on the pulsation frequencies were isolated by fixing the flame temperature through adjusting the amount of N_2 in air. Results show that the frequency increases with increasing intensities of the DL or DT instabilities, while the non-dimensional frequencies, normalized by the flame time, are collapsed and decrease as the flame becomes richer. Acceleration exponents of the global pulsation stage have been measured and found to be around 1.3, which is smaller than the suggested value of 1.5 for self-turbulization.

ACKNOWLEDGMENT

The work at Tsinghua University was supported by the National Natural Science Foundation of China 91841302. The work at Princeton University was supported by the US National Science Foundation (CBET, Grant # 1827287).

REFERENCES

[1] M. Matalon, Flame dynamics, Proceedings of the Combustion Institute, 32, 1 (2009).

[2] J. K. Bechtold and M. Matalon, Hydrodynamic and diffusion effects on the stability of spherically expanding flames, Combustion and Flame, 67, 1 (1987).

[3] M. Matalon, Intrinsic flame instabilities in premixed and nonpremixed combustion, Annual Review of Fluid Mechanics, 39, 1 (2007).

[4] S. Yang, A. Saha, F. Wu and C. K. Law, Morphology and self-acceleration of expanding laminar flames with flame-front cellular instabilities, Combustion and Flame, 171, (2016).

[5] C. K. Law, Combustion Physics, Cambridge University Press, 2006.

[6] D. M. Michelson and G. I. Sivashinsky, Nonlinear analysis of hydrodynamic instability in laminar flames—II. Numerical experiments, Acta Astronautica, 4, 11 (1977).

[7] G. I. Sivashinsky, Some developments in premixed combustion modeling, Proceedings of the Combustion Institute, 29, 2 (2002).

[8] J. K. B. R. Addabbo, M. Matalon, Wrinkling of spherically expanding flames, Proceedings in the Combustion Institude, 29, 2 (2002).

[9] D. Bradley, T. M. Cresswell and J. S. Puttock, Flame acceleration due to flame-induced instabilities in large-scale explosions, Combustion and Flame, 124, 4 (2001).

[10] W. K. Kim, T. Mogi, K. Kuwana and R. Dobashi, Self-similar propagation of expanding spherical flames in large scale gas explosions, Proceedings of the Combustion Institute, 35, 2 (2015).

[11] M. Z. Haq, Correlations for the Onset of Instabilities of Spherical Laminar Premixed Flames, Journal of Heat Transfer, 127, 12 (2005).

[12] C. K. Law, G. Jomaas and J. K. Bechtold, Cellular instabilities of expanding hydrogen/propane spherical flames at elevated pressures: theory and experiment, Proceedings of the Combustion Institute, 30, 1 (2005).

[13] G. Jomaas, C. K. Law and J. K. Bechtold, On transition to cellularity in expanding spherical flames, Journal of Fluid Mechanics, 583 (2007).

[14] F. Wu, G. Jomaas and C. K. Law, An experimental investigation on self-acceleration of cellular spherical flames, Proceedings of the Combustion Institute, 34, 1 (2013).

[15] Z.-Y. Sun, F.-S. Liu, X.-C. Bao and X.-H. Liu, Research on cellular instabilities in outwardly propagating spherical hydrogen-air flames, International Journal of Hydrogen Energy, 37, 9 (2012).

[16] J. Beeckmann, R. Hesse, S. Kruse, A. Berens, N. Peters, H. Pitsch and M. Matalon, Propagation speed and stability of spherically expanding hydrogen/air flames: Experimental study and asymptotics, Proceedings of the Combustion Institute, 36, 1 (2017).

[17] C. R. L. Bauwens, J. M. Bergthorson and S. B. Dorofeev, Experimental investigation of spherical-flame acceleration in lean hydrogen-air mixtures, International Journal of Hydrogen Energy, 42, 11 (2017).

[18] C. R. Bauwens, J. M. Bergthorson and S. B. Dorofeev, Experimental study of spherical-flame acceleration mechanisms in large-scale propane–air flames, Proceedings of the Combustion Institute, 35, 2 (2015).

[19] Y. X. Xin, C. S. Yoo, J. H. Chen and C. K. Law, A DNS study of self-accelerating cylindrical hydrogen–air flames with detailed chemistry, Proceedings of the Combustion Institute, 35, 1 (2015).

[20] C. Altantzis, C. E. Frouzakis, A. G. Tomboulides and K. Boulouchos, Numerical simulation of propagating circular and cylindrical lean premixed hydrogen/air flames, Proceedings of the Combustion Institute, 34, 1 (2013).

[21] J. L. Huo, A. Saha, Z. Ren and C. K. Law, Self-acceleration and global pulsation in hydrodynamically unstable expanding laminar flames, Combustion and Flame, 194 (2018).

[22] J. L. Huo, S. Yang, Z. Y. Ren, D. L. Zhu and C. K. Law, Uncertainty reduction in laminar flame speed extrapolation for expanding spherical flames, Combustion and Flame, 189 (2018).

[23] M. P. Burke, M. Chaos, Y. Ju, F. Dryer and S. J. Klippenstein, Comprehensive H2/O2 kinetic model for high□pressure combustion, International Journal of Chemical Kinetics, 44, 7 (2012).

[24] D. Bradley, R. A. Hicks, M. Lawes, C. G. W. Sheppard and R. Woolley, The Measurement of Laminar Burning Velocities and Markstein Numbers for Iso-octane–Air and Iso-octane–n-Heptane–Air Mixtures at Elevated Temperatures and Pressures in an Explosion Bomb, Combustion and Flame, 115, 1 (1998).

[25] C. R. L. Bauwens, J. M. Bergthorson and S. B. Dorofeev, Modeling the formation and growth of instabilities during spherical flame propagation, Proceedings of the Combustion Institute, DOI 10.1016/j.proci.2018.07.098 (2018).

[26] M. A. Liberman, M. F. Ivanov, O. E. Peil, D. M. Valiev and L.-E. Eriksson, Self-acceleration and fractal structure of outward freely propagating flames, Physics of Fluids, 16, 7 (2004).

[27] K. Mukaiyama, S. Shibayama and K. Kuwana, Fractal structures of hydrodynamically unstable and diffusive-thermally unstable flames, Combustion and Flame, 160, 11 (2013).

[28] Y. A. Gostintsev, A. G. Istratov, Y. V. Shulenin Self similar propagation of a free turbulent flame in mixed gas mixtures, Combust. Expl. Shock Waves, 24 (1988).